Int. J. Electrochem. Sci., 16 **(2021)** Article ID: 210336, doi: 10.20964/2021.03.03

International Journal of
ELECTROCHEMICAL
SCIENCE
www.electrochemsci.org

Corrosion Inhibition Effect of 5-Azidomethyl-8-Hydroxyquinoline on AISI 321 Stainless Steel in Phosphoric Acid Solution

Aimad Mazkour[1], Souad El Hajjaji[1,], Najoua Labjar[2], El Mostapha Lotfi[2], Mohammed El Mahi[2]*

[1] Laboratory of Spectroscopy, Molecular Modeling, Materials, Nanomaterials, Water and Environment, CERN2D, Faculty of Sciences, Mohammed V University in Rabat, Morocco
[2] Laboratory of Spectroscopy, Molecular Modeling, Materials, Nanomaterials, Water and Environment, CERN2D, ENSET, Mohammed V University in Rabat, Morocco
[*]E-mail: selhajjaji@hotmail.com or souad.elhajjaji@um5.ac.ma

Received: 20 September 2020 / *Accepted:* 4 November 2020 / *Published:* 31 January 2021

In the present paper, 5-Azidomethyl-8-hydroxyquinoline (AMHQ), a synthesized molecule, has been evaluated as a corrosion inhibitor for AISI 321 stainless steel in 5.5 M phosphoric acid solution, using chemical and electrochemical methods such as, hydrogen gas evolution, potentiostatic tests, potentiodynamic polarization, and impedance measurements (EIS). The obtained results show that the inhibition ability is enhanced with increasing concentrations of AMHQ and decreased with temperature. Potentiodynamic polarization curves showed that the AMHQ was acting as a mixed type inhibitor, by adsorption on both anodic and cathodic sites of Alloy 321. EIS measurements revealed that the dissolution of Alloy 321 is controlled by a mechanism of pure activation. The AMHQ is adsorbed on Alloy 321 surface according to the Langmuir isotherm adsorption model and thermodynamic parameters of the adsorption were also determined. Functional density theory (DFT) was used to modelize the interactions between the molecular structure of AMHQ and stainless steel surface.

Keywords: Corrosion; Inhibitor; Stainless steel; EIS; Phosphoric acid

1. INTRODUCTION

The phosphoric acid industry is a very aggressive environment towards materials that are used in the various stages of its manufacture (attack, filtration, concentration and storage). It is worth mentioning that ortho-phosphoric acid (H_3PO_4) is not aggressive enough when in its pure state, compared to other acids such as sulfuric acid, nitric acid and hydrochloric acid [1]. Moreover, the technology to produce phosphoric acid by wet process causes important corrosion-related damages due to the presence

of some undesirable impurities such as SO_4^{2-}, F^- and Cl^- [1].

Therefore, stainless steels are the materials of choice to guarantee a long operating time for the various installations in contact with phosphoric acid. Stainless steels are materials commonly used in many other applications such as food, chemical production, wastewater treatment plants and petroleum refining. Their corrosion resistance is due to the rapid growth of a stable, thin and extremely adherent layer, which protects metals against undesirable and destructive reactions with corrosive environments [2]. Although stainless steels are known for their excellent resistance compared to ordinary metals, the passive layer can be damaged under certain circumstances and corrosion can occur, especially in contact with a medium containing aggressive ions [1,2].

In terms of protection, the use of inhibitors is an efficient, original and easy-to-use method to protect metallic materials against corrosion in aggressive media.

Inhibitors for corrosion protection are substances that slow down or stop the corrosion process following their adsorption on the metal surface. Generally, the inhibitory properties depend to a large extent on the presence of heteroatoms and functional groups, its structure, its electronic properties and in particular at the donor sites, the aromaticity and the nature of π orbital donating electrons [3,4]. Many compounds can show great inhibitor efficiency, but their use is limited due to their toxicity to human health and the environment.

The study of stainless steels corrosion inhibition is still poorly mastered. Furthermore, as guidelines for the use of inhibitors are becoming more stringent in terms of ecology, the development of biodegradable and eco-friendly corrosion inhibitors is becoming a major issue.

AISI 321 stainless steel is a widely used alloy due to its mechanical and strength properties, high quality and weldability [5].

Hence, the objective of this study was to investigate the inhibition ability and the behavior of an eco-friendly synthesized molecule, 5-Azidomethyl-8-hydroxyquinoline (AMHQ), on the corrosion of AISI 321 stainless steel in 5.5 M phosphoric acid medium, by using chemical and electrochemical methods. An approach in chemical quantum computation was also conducted to highlight the relationship between the electronic structure of AMHQ and its corrosion inhibition performance.

2. MATERIALS AND METHODS

2.1. Material and test solution

Stabilized AISI 321 austenitic stainless steel (Alloy 321) was used in this study. The mass percentages of the additional elements other than iron (Fe) obtained by spectroscopic analysis were given in Table 1.

Table 1. Chemical composition of AISI 321stainless steel (Alloy 321) (wt.%).

Cr	Ni	C	Si	Mn	Ti	S	Mo	Cu	Nb
19.1	9.85	0.086	0.297	1.65	0.68	0.05	0.16	0.172	0.035

The used stainless steel samples were in a cylindrical shape with a surface area of 1 cm^2. An abrasive paper with different particle sizes (120-2000) was used to polish the samples, afterwards, the samples were degreasing and degassing in an ultrasonic bath containing ethanol, rinsed with distilled water and dried with warm air blower before being placed in the electrochemical cell.

The tests were conducted in a 5.5 M phosphoric acid solution with the addition of 2 wt.% H_2SO_4 and 0.06 wt.% KCl, from the dilution of commercial products, naturally ventilated and agitated. These concentrations were chosen to simulate the industrial phosphoric acid from Morocco's OCP Group (Cherifian Phosphate Office) [6]. Phosphoric acid was produced from Moroccan phosphate by wet process and the obtained acid contains about 40% wt of H_3PO_4 (5.5 M H_3PO_4) with some main impurities such as sulphates and chlorides. The measured pH value of the used phosphoric acid solution was 0.62.

2.2. The inhibitor molecule

The molecule used in this work as an inhibitor of Alloy 321 in phosphoric acid is 5-Azidomethyl-8-hydroxyquinoline (AMHQ), whose molecular structure is presented in Fig. 1. The synthesis method and the pharmaceutical properties of AMHQ following oral administration to mice were already reported [7-9].

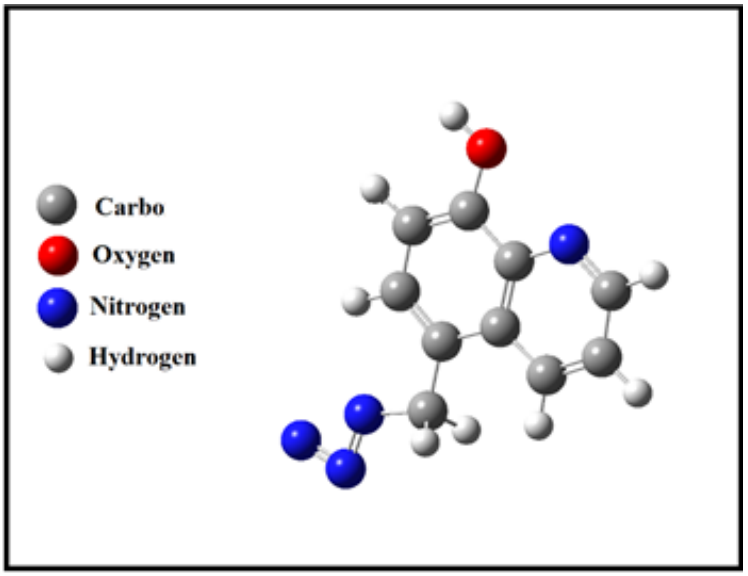

Figure 1. Molecular structure of 5-Azidomethyl-8-hydroxyquinoline.

2.3. Hydrogen evolution technique

The measurement of the hydrogen released during the corrosion process is considered a simple and reliable method to evaluate the protective performance of an inhibitor in acidic solutions. The conventional method of weight loss has certain disadvantages that sometimes make it difficult to interpret the results, especially when dealing with passivating materials. The measurements of the hydrogen evolution rate were carried out at 20°C using the simple assembly illustrated in Fig. 2.

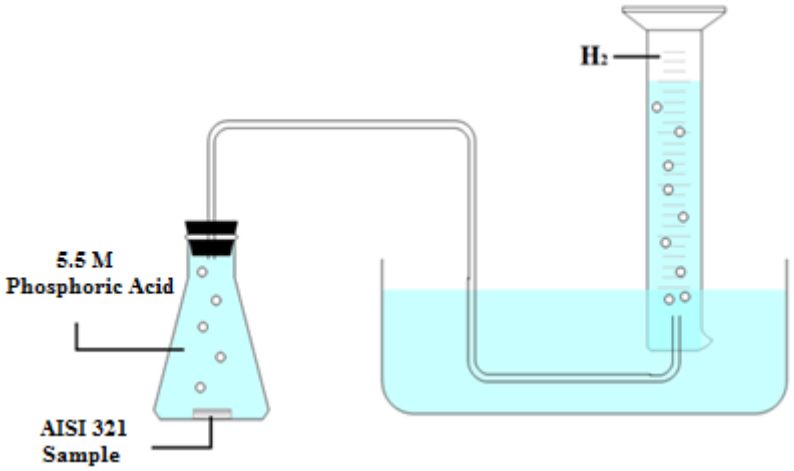

Figure 2. Illustration of the set-up for measuring the volume of hydrogen released.

The stainless steel sample was placed in an Erlenmeyer containing the acid solution. A pipe was used to connect the Erlenmeyer with an inverted graduated cylinder, mounted over a trough. The cylinder is initially filled with the acid solution. The hydrogen released from the sample entered the cylinder and progressively displaced the solution. Thus, the volume of hydrogen was easily measured by reading the position of the solution level in the graduated cylinder.

The inhibitor efficiency is directly calculated from the volume of hydrogen released by the following relation:

$$\%IE = \frac{V_0 - V_i}{V_0} \times 100 \qquad (1)$$

Where V_0 and V_i are the hydrogen gas released in the absence and the presence of the inhibitor respectively.

2.4. Electrochemical measurements

All the electrochemical experiments namely open circuit potential, polarization curves and electrochemical impedance spectroscopy (EIS) measurements, were performed in an electrochemical pyrex cell with three specific electrodes: a platinum auxiliary electrode, a second electrode (Cl | Hg_2Cl_2 (calomel) | Hg| Pt) as reference electrode and alloy 321 as a working electrode.

The measurements were carried out using a Biologic SP 150 Potentiostat-Galvanostat, controlled by EC-Lab V11.01 analysis software. The mechanical pre-treatment of the samples is insufficient to completely remove the oxide layer previously formed on the alloy surface. Therefore, the potential of -1 V/SCE was applied for 15 min before starting the electrochemical tests. The electrochemical behavior of AISI 321 sample in inhibited and uninhibited solutions was studied by recording anodic and cathodic polarization curves. The potential applied to the sample varies from -0.8 V/SCE to anodic potentials with a scan rate of 50 mV/min. Polarization data were treated using the EC-Lab V11.01 software and Tafel

extrapolation method was used to estimate corrosion current density values.

The Electrochemical impedance spectroscopy measurements (EIS) were performed after 60 minutes of immersion at the OCP potential in an aerated solution. EIS experiments have been recorded using a 10 mV root-mean-square perturbation from 10^5 to 10^{-2} Hz. The impedance diagrams are provided in Bode and Nyquist representations. The impedance curves fitting was carried out by the EC-Lab V11.01 analysis software. The tests were repeated several times to ensure good reproducibility of the results.

2.5. Quantum chemical study

In the last few years, quantum chemical methods have become a very effective tool for determining the molecular structure, and thus to highlight the relationship between the electronic properties of the inhibitor and its corrosion inhibition behavior. Therefore, it will be possible to control the inhibition mechanism by correlating the experimental results with those obtained theoretically [10-12].

The synthesized molecule was drawn using GaussView 5.0 software, and the standard Gaussian 09W software was used in quantum calculations after geometry optimization.

The correlation between AMHQ inhibition efficiency and their electronic properties was assessed by density functional theory (DFT) using B3LYP functional with 6-31G* basis set. The electrochemical corrosion phenomenon occurs in the aqueous phase, which requires taking into account the effect of the solvent in the theoretical calculations.

3. RESULTS AND DISCUSSION

3.1. Hydrogen evolution

The volume of hydrogen gas released on Alloy 321 surface versus time in the absence and the presence of various AMHQ concentrations was recorded at 20°C for about 48 h. Fig. 3 presents the effect of increasing concentration of AMHQ in 5.5 M phosphoric acid on the corrosion rate and consequently on the inhibition efficiency.

It is obvious that hydrogen gas evolved decreases markedly with the rise in the concentration of AMHQ, i.e. the corrosion inhibition is improved by increasing the inhibitor concentration and reaches a maximum value of about 94% for a concentration of $2.5 .10^{-2}$ mol/L. This behavior can be justified by the increase in AMHQ concentration which involves a growth in the surface of Alloy 321 covered by the inhibitor. This finding further confirms the fact that AMHQ effectively inhibited the corrosion of Alloy 321 in 5.5 M phosphoric acid.

The inhibition performance of AMHQ increases slightly over time, which may be the result of a displacement of the adsorption-desorption equilibrium in the forward direction and/or the growth of an oxide film on the Alloy 321 surface which becomes more stable and protective with the exposure time.

The immersion tests are easy to implement to evaluate inhibition efficiency. However, they give little data about the different mechanisms involved in the inhibition process.

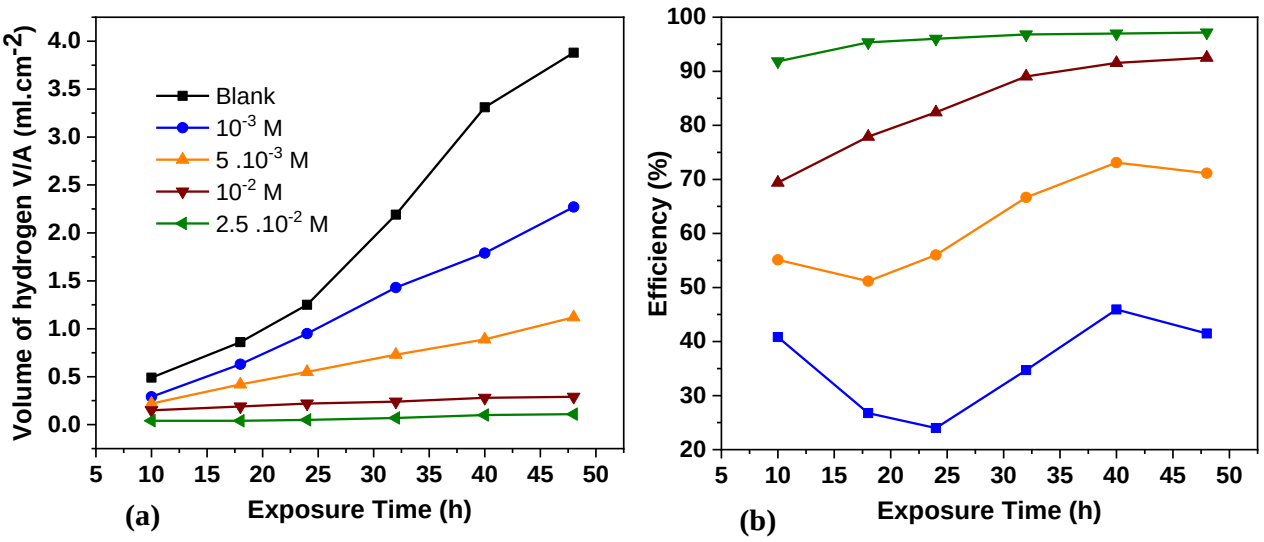

Figure 3. Evolution of hydrogen released (a) and the corresponding inhibition efficiencies (b) versus time of Alloy 321 in 5.5 M phosphoric acid with the addition of various concentrations of AMHQ at 20°C.

3.2. Open circuit potential versus time measurements

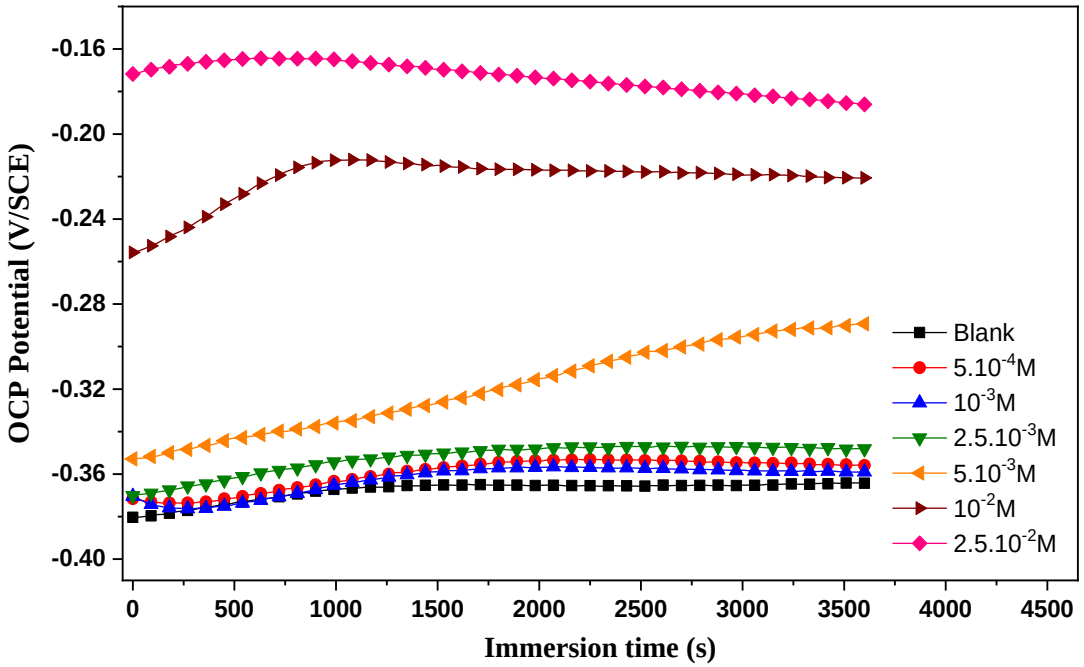

Figure 4. Evolution of the OCP versus time recorded of Alloy 321 in 5.5 M phosphoric acid without and with different concentrations of AMHQ at 20°C.

Open circuit potential (OCP) or mixed potential is the material potential without applying any external electrical charge. The evolution of OCP versus time can offer important qualitative information

about the processes at the metal / solution interface [13].

As indicated in the experimental part, the stability of the OCP took a particular importance before each electrochemical assay. Fig. 4 shows the evolution of the OCP of Alloy 321 versus time in 5.5 M phosphoric acid with the addition of various concentrations of AMHQ at 20°C.

The presence of AMHQ shifts the OCP potential towards more anodic values for all concentrations. The ennobling of OCP value indicates a change of the oxide layer grown on the metal surface and its thickening following the interaction between the phosphoric acid solution and Alloy 321. Oxide film growth continues until a stable thickness in the electrolyte is reached [14]. Alloy 321 contains a percentage of 19.1 of chromium, which ensures the development of a passive layer on its surface. Thus, during the OCP assay, chromium oxide grows on the surface of the electrode, shifting the OCP value to more positive potentials [6].

Fig. 4 exhibits a positive correlation between the steady-state potential and the concentration of AMHQ. The increase in AMHQ concentration implies an enhancement of the OCP value. The positive OCP displacement in the presence of AMHQ suggests that the inhibitor can prevent corrosion of alloy 321 by mainly control the anodic process. In acidic environments, the oxidation of alloys and alloying elements constitutes the anodic reaction, while the cathodic reaction involves H^+ reduction to produce hydrogen gas and/or oxygen reduction. The action of inhibitors results in a decrease in the rate of one or both anodic and cathodic reactions [15].

3.3. Potentiodynamic polarization measurements

In order to highlight the mechanisms and kinetics of alloy 321 corrosion, as well as the changes made following the addition of the inhibitor, the samples were cathodically and anodically polarized to plot potentiodynamic polarization curves.

The current-potential relationships of Alloy 321 in 5.5 M phosphoric acid with various concentrations of AMHQ are presented in Fig. 5.

Electrochemical data extracted from the polarization curves including mixed potential (E_{corr}), corrosion current density (I_{corr}), critical current density (I_{crit}), passivation current density (I_{pas}) and inhibition efficiency (E%) are summarized in Table 2. The inhibition efficiency values are calculated from the polarization parameters using the following relation:

$$E\% = [(I^{\circ}_{corr} - I_{corr}) / I^{\circ}_{corr}] \times 100 \qquad (2)$$

Where I°_{corr} and I_{corr} are the corrosion current density values without and with addition of AMHQ, respectively.

It should be noted that the occurring of the active-passive transition on the anodic zone of such curves, restricts the potential interval for the linear behaviour of Tafel, which makes it difficult to accurately specify the corresponding Tafel tangent. However, the extrapolation of the cathodic reduction must be sufficient to determine the corrosion current density by extrapolation of Tafel to the abandon potential [16,17]. This oncoming would provide the net value of the cathodic process rate to the abandon potential. It is as well the net value of the anodic reaction rate to abandon potential that has been checked by other non-electrochemical methods [18].

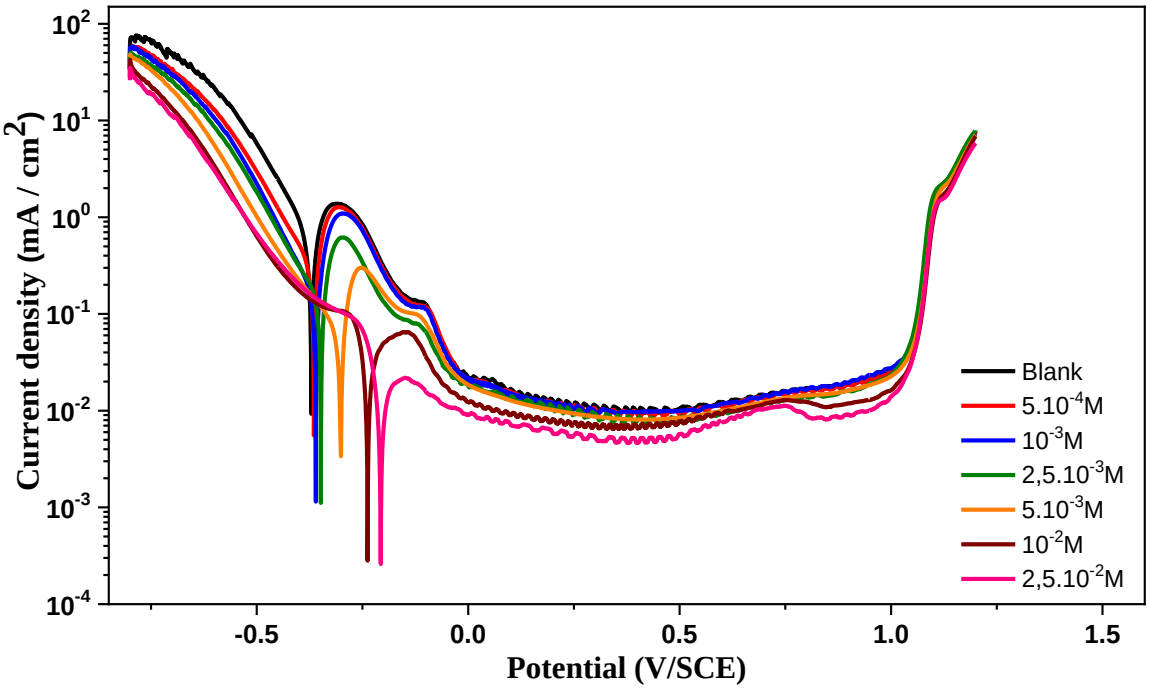

Figure 5. Polarization curves of Alloy 321 in 5.5 M phosphoric acid with various AMHQ concentrations at 20°C.

The potentiodynamic polarization curves, with and without inhibitor, show a wide range of passivity (around 1V), to which current density remains more or less stable. The low current passivity indicates that Alloy 321 has good resistance towards this media, this current slightly decreases in the presence of AMHQ.

Table 2. Electrochemical data of Alloy 321 in 5.5 M phosphoric acid at different concentrations of AMHQ.

Concentration (M)	E_{corr} (mV/SCE)	i_{corr} (uA.cm^{-2})	i_{pas} (uA.cm^{-2})	i_{crit} (mA.cm^{-2})	Efficiency %
Blank	-377	384.07	7.61	1.163	-------
5.10^{-4}	-365	317.20	7.71	0.847	17
10^{-3}	-361	272.73	8.01	0.729	28
2.5.10^{-3}	-350	176.80	8.15	0.411	53
5.10^{-3}	-302	84.20	7.09	0.200	78
10^{-2}	-233	28.47	6.28	0.043	93
2.5.10^{-2}	-204	6.00	4.82	0.014	98

The polarization curves in Fig. 5 show that the addition of AMHQ decreases the anodic oxidation and retards H^+ reduction on Alloy 321 cathodic areas. For AMHQ concentrations less than 5.10^{-3} M, the cathodic curves evolve exponentially to Tafel lines suggesting that the hydrogen reduction at AISI 321 surface occurs by a pure activation mechanism [19]. However, when the AMHQ concentration exceeds 5.10^{-3} M, a diffusion plateau begins to appear reflecting the oxygen diffusion from the aerated solution to the interface.

It is also worth mentioning that the presence of AMHQ induced a gradual disappearance of the active passive transition of the metal, thus supporting the formation of an oxide film, which resulted in a more stable oxide range and lower dissolution of the oxide as shown. All these results confirm the fact that AMHQ is a mixed type inhibitor of Alloy 321 in 5.5 M phosphoric acid.

The data presented in Table 2 show that increasing AMHQ concentration decreases the corrosion current density (I_{corr}) and increases the inhibition efficiency which reaches a maximum value of 99% at $2.5.10^{-2}$ M of inhibitor. The corrosion potential shift towards more anodic values in the presence of AMHQ shows that the inhibitory effect is predominant in the anodic process, and also confirms the passivating character of the inhibitor.

3.4. Electrochemical impedance spectroscopy (EIS)

To define the changes induced by the addition of AMHQ at the interface AISI 321 /5.5M H_3PO_4 and to investigate the stability of the passive film grown on AISI 321 surface, an impedance analysis was conducted. Nyquist and Bode plots of AISI 321 were plotted under potentiostatic conditions after 60 minutes of immersion in 5.5 M phosphoric acid in the absence and the presence of AMHQ. The results are illustrated in Fig. 6 and 7.

Nyquist diagrams in Fig. 6 exhibit single imperfect and depressed semicircles over the frequency range, indicating that Alloy 321 dissolution is monitored by a charge-transfer process on a heterogeneous area [20]. An increase in the capacitive half-loop size is observed with the rise of the inhibitor concentration, indicating that the inhibition performance is a function of AMHQ concentration. This can be the consequence of the adsorption and the reinforcement of an inhibiting film on AISI 321 surface [21].

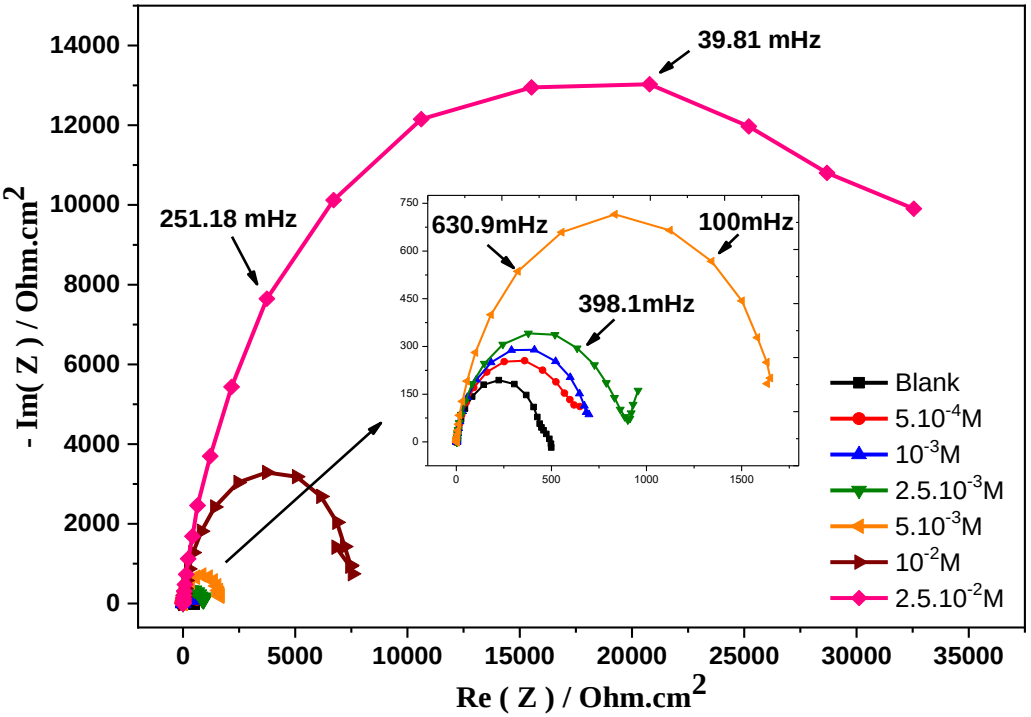

Figure 6. Nyquist diagrams of Alloy 321 after one hour of immersion at OCP potential in inhibited and uninhibited solutions of 5.5 M phosphoric acid at 20°C.

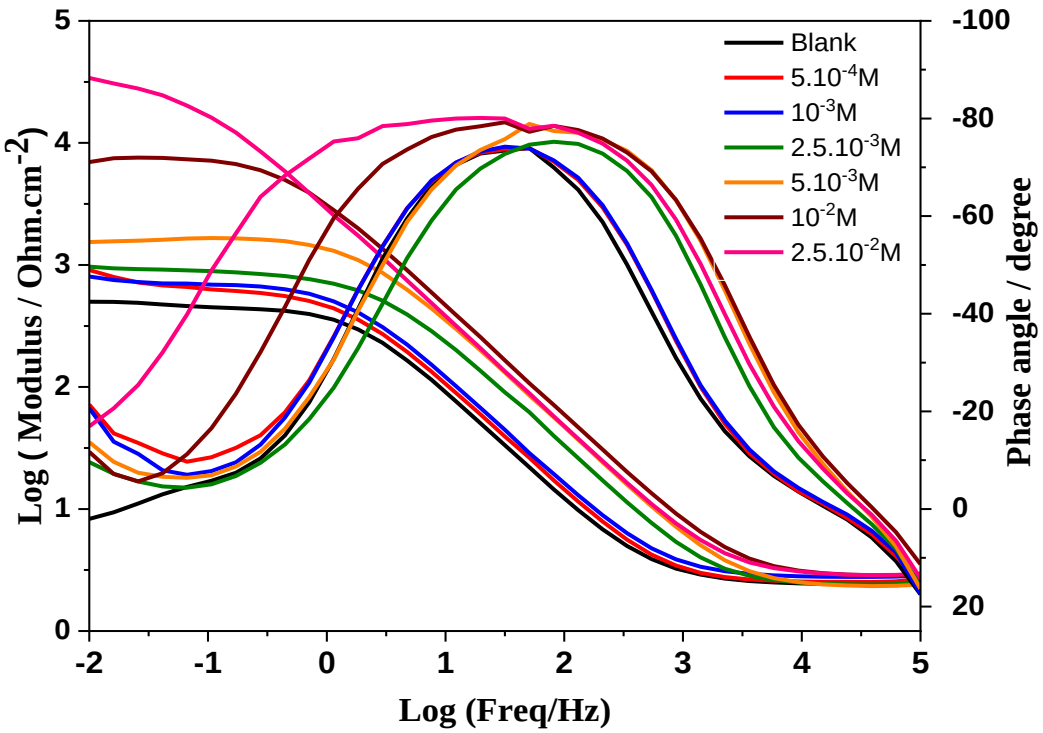

Figure 7. Bode plots of Alloy 321 after one hour of immersion at OCP potential in inhibited and uninhibited solutions of 5.5 M phosphoric acid at 20°C.

To better exploit impedance analysis, a fitting procedure was implemented using electrical equivalent circuits.

From Bode diagrams and for concentrations less than 10^{-2} mol/L, only one-time constant is distinguished across the studied frequency range in θ = f (Frequency) plots. Therefore, a simple Randles circuit (Fig. 8a) consisting of an uncompensated solution resistance (Rs) and a constant phase element (CPE) in parallel to a faradic resistance R_F was used. In the case of 2.5 .10^{-2} mol/L of inhibitor, a Warburg element is added in series with the faradic resistance (Fig. 8b), indicating the dominance of the oxygen diffusion process in the low frequencies. An excellent fitting of EIS data was found with a coefficient χ2 of the order of 10^{-3} using the circuits mentioned below.

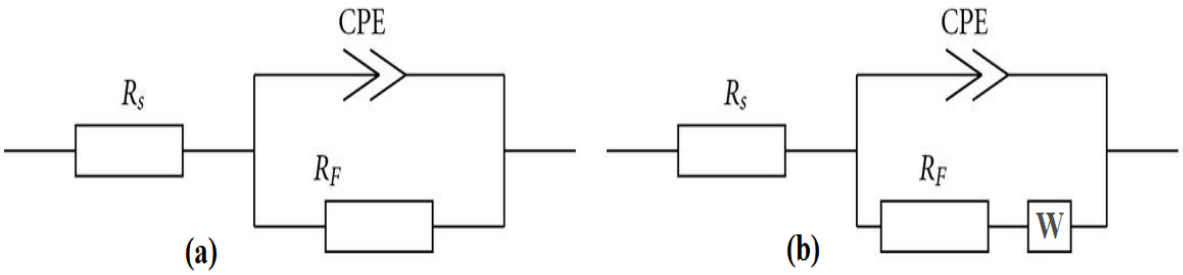

Figure 8. The equivalent electrical circuits used to model the experimental data. (a) for EIS measurements at concentrations from 5 .10^{-4} M to 10^{-2} M ; (b) for EIS measurements at 2.5 .10^{-2} M.

The theoretical parameters resulting from the adjustment of the impedance curves using the electrical circuits are presented in Table 3. The following relation is used to estimate the inhibitor efficiency:

$$E\% = [(R_{ct} - R^{\circ}_{ct}) / R_{ct}] \times 100 \qquad (3)$$

Where R_{ct} and R°_{ct} are the charge-transfer resistances in the presence and the absence of AMHQ respectively.

Table 3. Impedance data of Alloy 321 in inhibited and uninhibited solutions of 5.5 M phosphoric acid solution.

Concentration (M)	Rs ($\Omega.cm^2$)	R_F ($\Omega.cm^2$)	Q. 10^{-6} ($\Omega^{-1}.cm^{-2}.s^n$)	n	W_d ($\Omega.s^{-1/2}$)	Efficiency %
Blank	2.452	466.5	254	0.86	-------	---------
5.10^{-4}	2.496	671.3	239	0.86	-------	31
10^{-3}	2.761	712.5	170	0.87	-------	35
2.5.10^{-3}	2.367	882.7	97	0.89	-------	47
5.10^{-3}	2.306	1626	62	0.91	-------	71
10^{-2}	2.824	7589	51	0.91	-------	94
2.5.10^{-2}	2.841	32785	26	0.93	1480	99

All θ = f (Frequency) curves are less than 90°, which can be interpreted as an ideal capacitor

deviation behavior. Therefore, a CPE element (constant phase element) was used to simulate the non-ideal behavior of the capacitive elements, which is attributed to several factors including the surface inhomogeneity and roughness, the adsorption of compounds, dislocations, grain boundaries, the formation of porous layers and the presence of impurities [1,6]. The impedance of this element is defined as:

$$Z_{cpe} = A^{-1}(i\omega)^{-n} \qquad (4)$$

Where A is the general induction function, $\boldsymbol{\omega}$ symbolizes the angular frequency (in rad/s), $i^2 = -1$ is the imaginary number and n is the phase shift-related coefficient [1]. When the n value is equal to 0.5, -1, 0 and 1, the CPE element is reduced respectively to a Warburg impedance (W), an inductor (L), resistance (R) and a plane capacitor (C).

The examination of the results shows that the inhibition efficiency becomes more important with the rise of AMHQ concentration and reaches a value of 99% for $2.5 .10^{-2}$ mol/L of inhibitor, in agreement with the outcomes of hydrogen evolution method and those of the polarization curves.

The solution resistance at high frequency remains almost constant by the addition of AMHQ. This finding shows that the inhibitor does not induce significant changes in the physicochemical parameters of the solution and thus satisfies one of the requirements for the practical use of the inhibitors.

It can be seen that as AMHQ concentration rises, the double layer capacitance decreased, while the faradic resistance increased reflecting the protecting character of the added inhibitor. The lowering of double layer pseudo-capacitance may be due to the decrease of the local dielectric constant and / or the thickening of the electrical double layer, conforming to the expression of the double layer capacity presented in the Helmholtz model [22]:

$$C = \varepsilon\varepsilon_0 \frac{S}{e} \qquad (5)$$

Where ε_0 is the vacuum permittivity (8.8542×10^{-14} F/cm), ε is the relative dielectric constant of the layer, e is the thickness of the dielectric in m and S is the surface area in m^2.

These results suggested that AMHQ molecule acted by adsorption at the Alloy 321/5.5 H_3PO_4 interface [23]. The low value of n indicates that the surface of alloy 321 is relatively heterogeneous and rough due to the corrosion reaction. The addition of AMHQ induced an increase in n value (from 0.86 to 0.93) meaning an improvement in surface homogeneity due to the absorption of AMHQ on the metal surface.

When the n value is greater than 0.8 (between 0.8 and 1), the CPE behavior (Q) approaches to a pure capacitance (C) of the film formed on the stainless steel surface [24].

The change of the internal oxide film composition produced by the alloying elements [25,26] leads to considering the Power Law model announced by Orazem et al. [27] to correlate the parameters of the CPE with the physical properties of the oxide films and characterize their volume inhomogeneities. The use of this model justifies the empirical use of an R / Q circuit to modelize the passive film. Furthermore, it allows calculating the oxide film thickness [28] through the determination of the profile taking into account the variation in resistance with thickness [27,29].

According to this model, the CPE element is converted into a pure capacitance (C) using the following relation:

$$C_{eff} = gQ(\rho_\delta \varepsilon\varepsilon_0)^{1-n} \qquad (6)$$

And the film thickness could be estimated using the following relation:

$$\delta = ((\varepsilon\varepsilon_0)^n)/(g\rho_\delta^{1-n}Q) \quad (7)$$

Where ε and ε_0 are previously defined. According to the literature and for the case of oxide film formed on stainless steel, values of 15.6, 500 and $1 + 2.88(1 - n)^{2.375}$ are usually attributed to ε, ρ_δ and g respectively [30,31].

Values of C_{eff} and δ are presented in Table 4. The calculated values of passive film thickness are similar to those found by other methods such as XPS.

Table 4. Effective capacitance and thickness values of passive films formed on the Alloy 321 in inhibited and uninhibited solutions of 5.5 M phosphoric acid.

Concentration (M)	Q. 10^{-6} ($\Omega^{-1}.cm^{-2}.s^n$)	N	C_{eff} ($\mu F.cm^2$)	δ (nm)
Blank	254	0.86	13.61	1.01
5.10^{-4}	239	0.86	12.8	1.08
10^{-3}	170	0.87	11.2	1.23
$2.5.10^{-3}$	97	0.89	9.77	1.43
5.10^{-3}	62	0.91	9.38	1.47
10^{-2}	51	0.91	7.71	1.79
$2.5.10^{-2}$	26	0.93	5.97	2.31

The theoretical thickness values of the oxide films formed on Alloy 321 in inhibited and uninhibited solutions of 5.5 M phosphoric acid are between 1.01 and 2.31 nm. These thickness values are of the same order of magnitude as those found by other authors for austenitic stainless steels in acidic media [32]. The thickness of the film formed on Alloy 321 surface increases with elevating AMHQ concentration. The addition of AMHQ and its adsorption on the Alloy 321 surface have allowed the development of a thicker, more stable and more protective layer which constitutes an effective barrier against corrosion processes.

3.5. Adsorption isotherm

The adsorption of an inhibitor on the metal surface determines its efficiency and depends on several factors such as the molecular and electronic structure of the inhibitor, the metallic facial charge and the nature of the solvent. Therefore, adsorption isotherms are very important in describing the mode of adsorption of inhibitors on the metal surface according to their concentrations [33]. The most commonly employed adsorption models in the corrosion inhibition study are Langmuir, Freundlich, Flory Huggins, Temkin and Frumkin isotherms [34]. Assuming that AMHQ inhibits the corrosion reaction by a non-reactive blockage of AISI 321 surface, and the inhibitor intervenes only by subtracting a portion of the surface from both anodic and cathodic reactions (mixed type inhibitor), the inhibition efficiency represents is a direct measure of the surface coverage (θ).

$$\theta = 1 - \frac{i_{inh}}{i_o} = \frac{E\%}{100} \quad (8)$$

Attempts to adjust the surface coverage values with the corresponding concentrations using the different adsorption isotherms reveal that the Langmuir adsorption isotherm was the most appropriate to explain the adsorption behavior of AMHQ on AISI 321 in 5.5 M phosphoric acid.

The linearity of the graph $C_{inh}/\theta = f(C_{inh})$ (Fig. 9) ($R^2 \approx$ Slope ≈ 1) indicate that the adsorption of AMHQ on Alloy 321 surface obeys the adsorption isotherm of Langmuir modeled by the following equation:

$$\frac{C_{inh}}{\theta} = \frac{1}{K_{ads}} + C_{inh} \qquad (9)$$

Where C_{inh} is the inhibitor concentration in the electrolyte and K_{ads} is the equilibrium constant of the adsorption/desorption process.

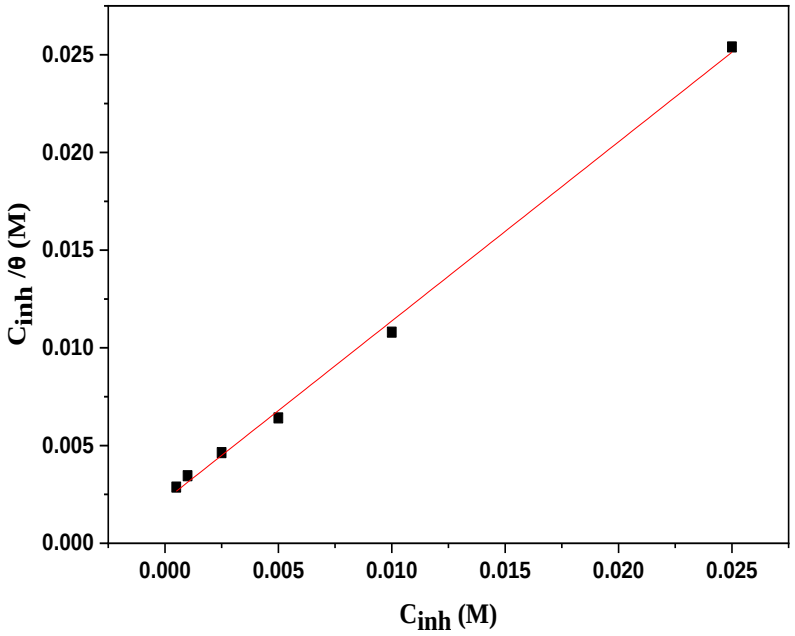

Figure 9. Langmuir adsorption isotherm of AMHQ on Alloy 321 surface in 5.5 M phosphoric acid solution.

The adsorbent metal is commonly modeled by a solid surface composed of several distinct sites capable of binding the inhibitor (adsorbate). The adsorption process is considered as a chemical reaction between the inhibitor and an active site, with a binding that can be either electrostatic or chemical. This reaction leads to an adsorbed complex [Molecule-Metal surface] with an associated equilibrium constant K_{ads}.

The Langmuir adsorption isotherm assumes that AMHQ is adsorbed to the Alloy 321 surface, and covers the surface as a monolayer of adsorbed inhibitors. The adsorbed inhibitor molecules are immobile, do not interact with each other and each molecule occupies a particular active site which can be either anodic or cathodic as shown by the polarization curves.

Gibbs energy of adsorption process $\Delta G°_{ads}$ can be obtained from the adsorption–desorption equilibrium constant value (K) using the following relation:

$$K = \frac{1}{55.5} \exp(\frac{\Delta G^0_{ads}}{RT}) \quad (10)$$

Where T is the solution temperature in Kelvin (K), R=8.314 $J.K^{-1}.mol^{-1}$ is the molar gas constant, 55.5 is the water concentration, $\Delta G°_{ads}$ is the adsorption Gibbs free energy and K_{ads} is the equilibrium constant of the adsorption–desorption process.

The free adsorption energy $\Delta G°_{ads}$ is negative (Table 5), which indicates that the adsorption of AMHQ on the surface of Alloy 321 is a spontaneous process and reflects the stability of the adsorbed complex [35].

Table 5. Thermodynamic parameters of the Alloy 321 corrosion process in 5.5 M phosphoric acid in the absence and the presence of different concentrations of AMHQ.

Linear correlation (coefficient R^2)	Slope	K (M^{-1})	$\Delta G°_{ads}$ ($KJ.mol^{-1}$)
0.998	0.92	454.54	- 24.8

Furthermore, $\Delta G°_{ads}$ absolute values less than 20 Kj/mol are correlated with the electrostatic interaction between the inhibitors and the metal (physisorption), while values greater than 40 Kj/mol involve the formation of strong bonds by transfer or sharing electrons between the inhibitor molecules and the alloy surface (chemisorption) [36]. Accordingly, the absolute value of the calculated $\Delta G°_{ads}$ (24.8 Kj/mol) lies between 20 and 40 Kj/mol indicate the presence of a strong bond between AMHQ and the surface of Alloy 321, and the interaction implies both chemisorption and physisorption with a dominance of physisorption interactions [37].

3.6. Corrosion inhibition mechanism

It is worth mentioning that, in acidic solutions, organic inhibitor compounds can be protonated, i.e. they can exist in their cationic form [38].

$$[AMHQ] + n\,H^+ \rightleftharpoons [AMHQH_n]^{n+} \quad (1)$$

Therefore, in acid medium, both cationic and neutral forms of the inhibitor molecule can exist. According to previous studies, the adsorption of molecules depends mainly on its total charge and the surface charge of metal. The inner potential Φ of a metal determines its surface charge, which is the difference between the mixed potential (E_{corr}) and the zero charge potential (PZC) [39].

$$\Phi = E_{corr} - PZC \quad (11)$$

The PZC is a potential characterizing each electrochemical interface where the solution / metal interface has no charge and the double layer no longer exists. EIS was used to evaluate the zero-charge potential.

The EIS experiments were carried out by scanning the applied operating potential (anodic and cathodic potentials) excluding the OCP potential. The faradic resistance and capacitance values are recorded and plotted against the applied potentials. These two curves represent a maximum and a

minimum which must correspond to the same potential called PZC.

Fig. 10 shows the evolution of the polarization resistance and capacitance according to the applied potentials of Alloy 321 in 5.5 M phosphoric acid with 10^{-2} M of AMHQ.

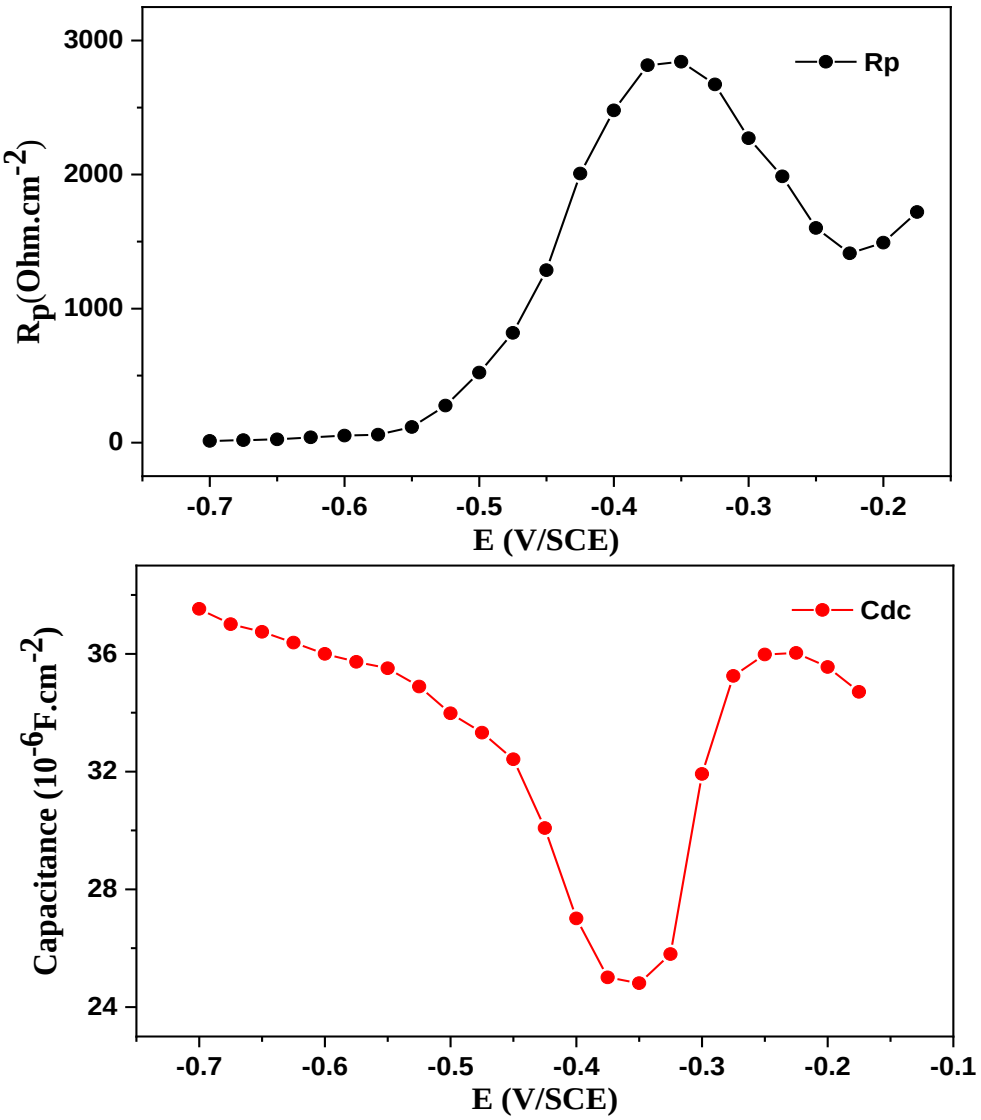

Figure 10. Evolution of the polarization resistance and the capacitance as a function of the applied potential of Alloy 321 in 5.5 M phosphoric acid with 10^{-2} M of AMHQ.

From Fig. 10, The PZC value is approximately -356 mV for both curves. The mixed corrosion potential of Alloy 321 in the same conditions was -225 mV. As a result, the inner potential is -225-(-356) = 131 mV, which indicates that the metal surface is positively charged in comparison to its PZC.

Therefore, the chloride and sulfate ions (anions) in the solution will undergo an electrostatic attraction (Physical adsorption) towards the positively charged metal surface and will form the primary adsorbed layer of anions on the oxide film. In our case of Alloy 321, chromium and nickel exist in the passive film as (Cr_2O_3) and (NiO) [38]. After this first anions adsorption, the electrode surface will

become negatively charged, therefore, the protonated inhibitor molecules will be attached with the first adsorption layer by physical interaction (Fig. 11).

Furthermore, AMHQ neutral molecules could be adsorbed on Alloy 321 surface by a chemisorption mechanism, implying the displacement of water molecules from the Alloy surface and the sharing electrons through its active sites [39].

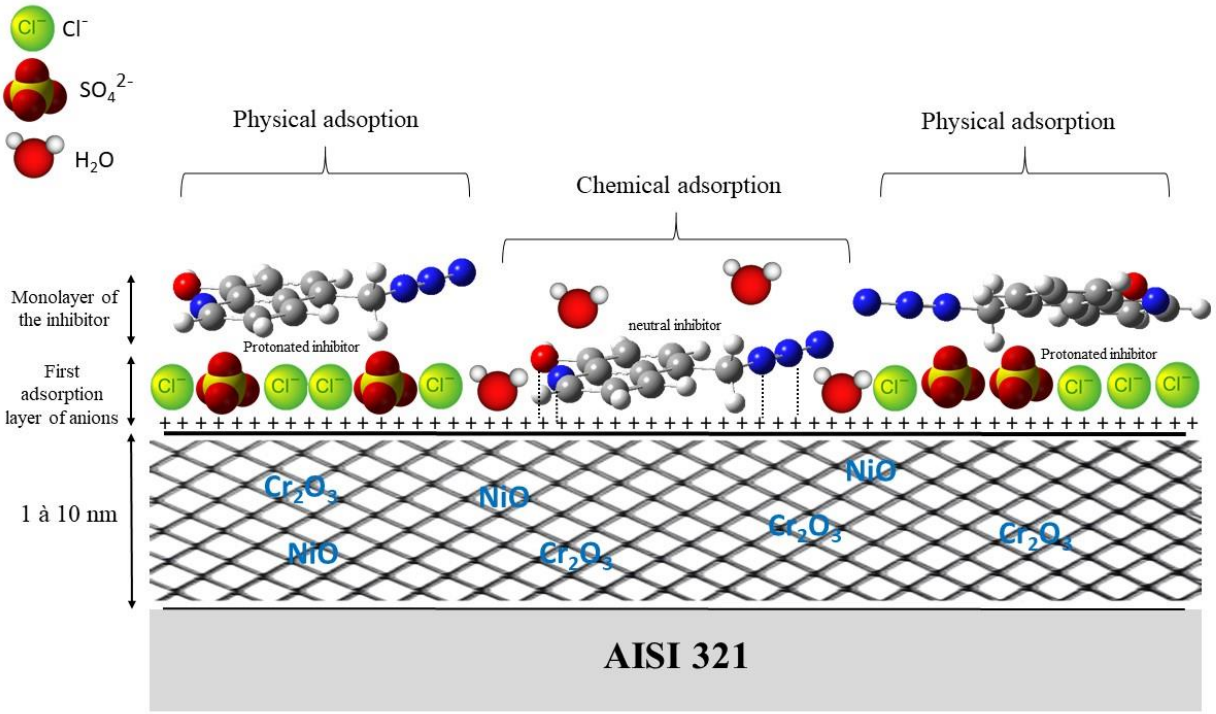

Figure 11. General proposed mechanism of corrosion inhibition of AMHQ on Alloy 321 in 5.5 M phosphoric acid.

3.7. Temperature effect

In order to investigate the influence of elevating phosphoric acid temperature on the inhibition action of AMHQ against Alloy 321 corrosion, polarization curves were realized at various temperatures ranging from 20 to 60°C in the absence and in the presence of 10^{-2} mol/L of inhibitor after one hour of immersion (Fig. 12). The corresponding data are shown in Table 6.

For all temperatures, the polarization curves of Alloy 321 in 5.5 M phosphoric acid retain almost the same general shape, with a wide range of passivity. It's obvious from Fig. 12 (a) that elevating acid temperature affects in the same time the cathodic and anodic reactions. The temperature rise enhances the reduction of H^+ and implies an increase of the passive current density. The transpassive potential value remains almost constant even with the harmful effect of the chloride favored by the temperature rise.

In the presence of AMHQ, a diffusion plateau is observed between -0.41 V/SCE and E_{corr} indicates that the oxygen reduction contributes to the increase of the cathodic current with temperature.

The tests were carried out in an aerated cell without agitation. It is well known that the oxygen concentration decreases with the temperature rise. However, the diffusion coefficient of oxygen is increased with temperature inducing a higher cathodic current density [1].

At higher temperature (50 - 60°C), the cathodic and anodic currents intersect at three points. Such a form of polarization curve is commonly observed with corrosion resistant alloys. At low potentials, the curve shape is similar to that shown in law temperature. Above the active pic, a second E_{corr} appears followed by a "loop" and also a third E_{corr} before the passive region is reached [40].

The appearance of the cathodic loop in this case can be explained by the fact that at this potential range, the passive current is lower than the cathodic reaction rate. Thus, the effective net current at these potential values is the cathodic current [40].

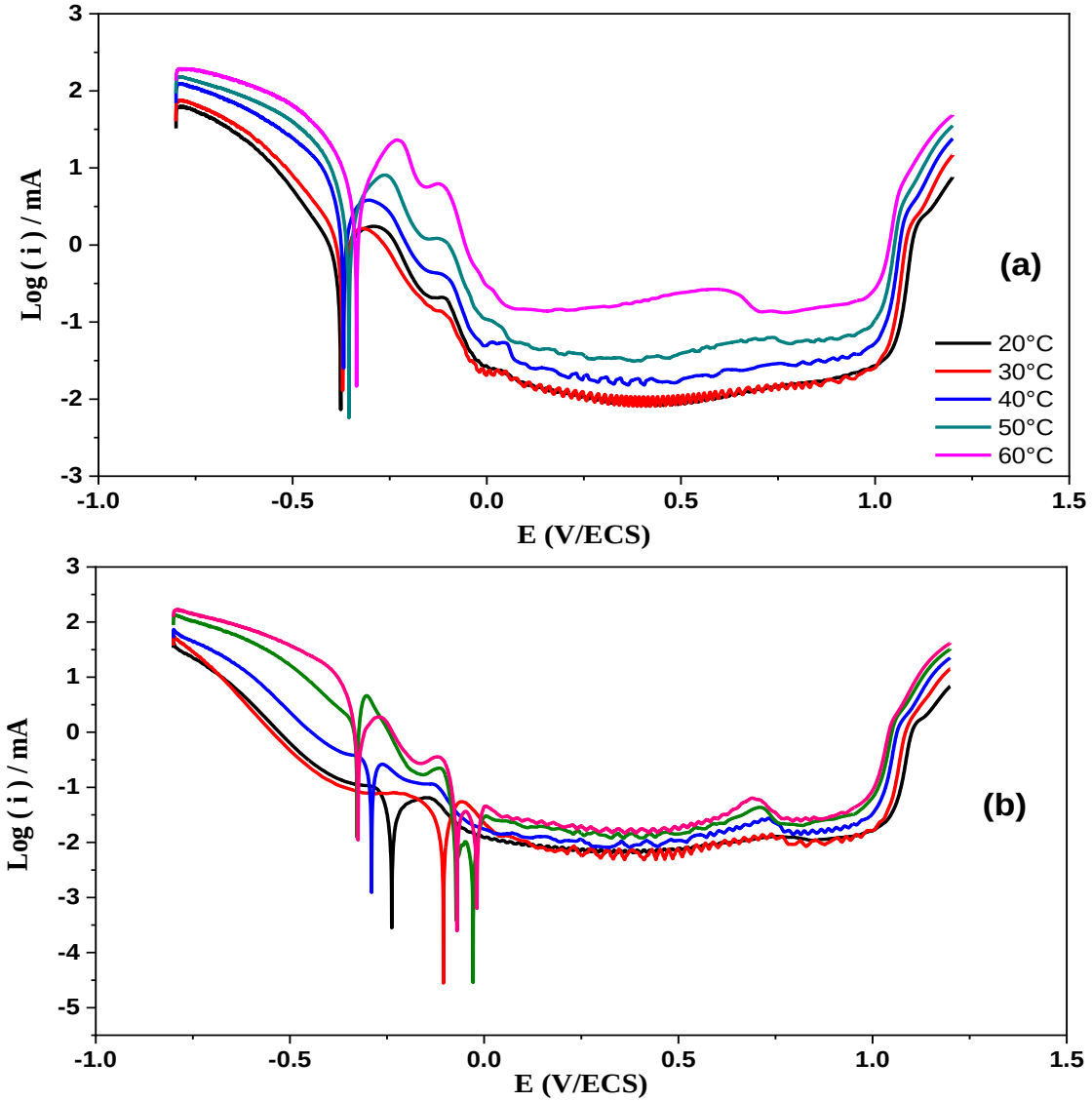

Figure 12. Temperature effect on potentiodynamic polarization curves of Alloy 321 in uninhibited (a) and inhibited (b) acid solutions.

Table 6. Corrosion parameters of Alloy 321 in 5.5 M phosphoric acid in the absence and the presence of 2.2 .10^{-2} mol/L of inhibitor at different temperatures.

Temperature (°C)	I_{corr} (µA/cm²)		Efficiency (%)
	H_3PO_4 5.5 M	10^{-2} M of inhibitor	
20	384.07	28.47	93
30	406.33	32.07	92
40	745.53	146.2	80
50	975.73	437.53	55
60	1671.6	851.87	49

The inhibition efficiency of AMHQ on Alloy 321 in phosphoric acid decreased with increasing acid temperature from 20 to 60°C. This indicates that AMHQ desorption is favored by elevating acid temperature. This finding confirms that the inhibition takes place by a predominantly electrostatic adsorption of AMHQ on the Alloy 321 surface. The activation indices of Alloy 321 dissolution process were obtained from the Arrhenius plot using the following relation:

$$I_{corr} = A\exp\left(-\frac{E_a}{RT}\right) \qquad (12)$$

Where T is the temperature in Kelvin (K), R is the universal gas constant, E_a is the activation energy of the corrosion reaction, A is the Arrhenius pre-exponential factor.

The E_a values of Alloy 321 in 5.5 M phosphoric acid without and with 10^{-2} M of AMHQ are estimated from the slope of the graph log I_{corr} = f (T^{-1}) (Fig. 13). The results are shown in Table 7.

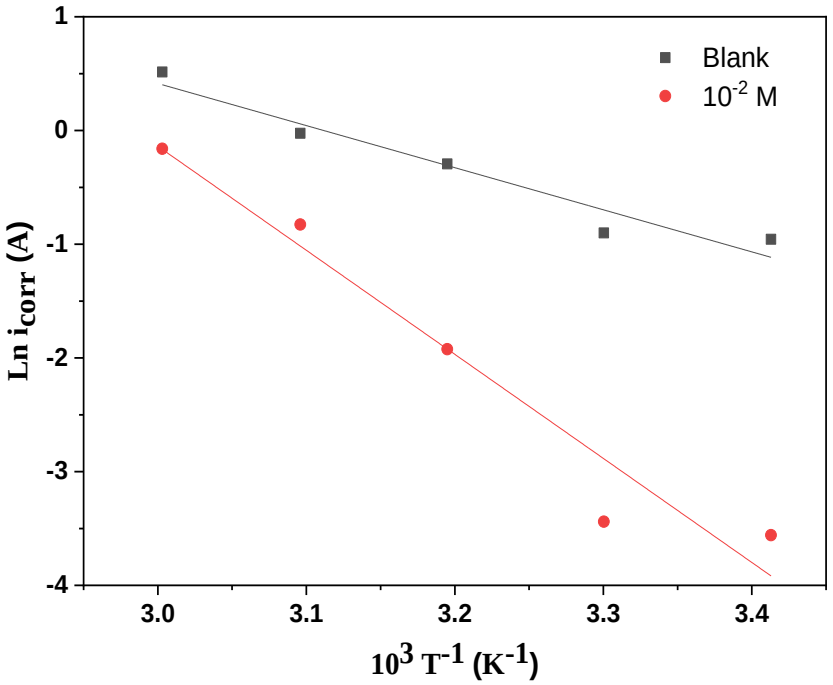

Figure 13. Arrhenius plots of Alloy 321 in 5.5 M phosphoric acid without and with the addition of 10^{-2} M of AMHQ.

Table 7. Thermodynamic parameters of Alloy 321 dissolution in 5.5 M phosphoric acid without and with the addition of 10^{-2} M of AMHQ.

Inhibitor	E_a ((kJ.mol^{-1}))	$\Delta H°_a$ (kJ.mol^{-1})	$\Delta S°_a$ (J .mol^{-1})	$E_a - \Delta H°_a$ (kJ.mol^{-1})
H_3PO_4 5.5 M	30.78	28.18	-157.85	2.6
H_3PO_4 5.5 M + 10^{-2}M of inhibitor	76.08	73.49	-26.52	2.59

A linear variation of Ln i_{corr} = f (1 / T) is observed, which means the implication of an active process. Activation energy is defined as the energy that requires a reagent to generate the products. E_a value of Alloy 321 in 5.5 M phosphoric acid with the presence of AMHQ is higher than that for the uninhibited solution, which indicates that the dissolution of the material in the presence of the inhibitor is slow and more exigent in terms of energy [41]. This may be justified by the fact that the presence of AMHQ induces an energy barrier for the corrosion process and the energy barrier increases with increasing concentration of AMHQ.

The increase in activation energy can be justified by the electrostatic adsorption of AMHQ which occurs on Alloy 321 surface. It has been reported that the decrease in the inhibitor adsorption on the metal surface with increasing acid temperature is responsible for elevating the activation energy [42]. Since the desorption is in equilibrium with the adsorption process, the desorption of the inhibitor molecules is favored when the adsorption decreases. The decrease in the adsorption of inhibitor molecules at high temperature leads to the restriction of the stainless steel surface covered by the inhibitor, and therefore to the increase in the oxidation rate [42].

The transition state plots of log I_{corr}/T = f (1/T) (Fig. 14) of Alloy 321 dissolution in 5.5 M phosphoric acid without and with the addition of 10^{-2} M of AMHQ was exploited to estimate thermodynamic parameters including entropy of activation ($\Delta S°_a$) and enthalpy of activation ($\Delta H°_a$) using the following Equation:

$$I_{corr} = \frac{RT}{N_a h} \exp\left(\frac{\Delta S°_a}{R}\right) \exp\left(-\frac{\Delta H°_a}{RT}\right) \qquad (13)$$

Where T is the temperature in Kelvin, R is the molar gas constant, N_a is Avogadro's constant, h is the plank's constant, $\Delta H°_a$ is the apparent enthalpy of activation and $\Delta S°_a$ is the apparent entropy of activation.

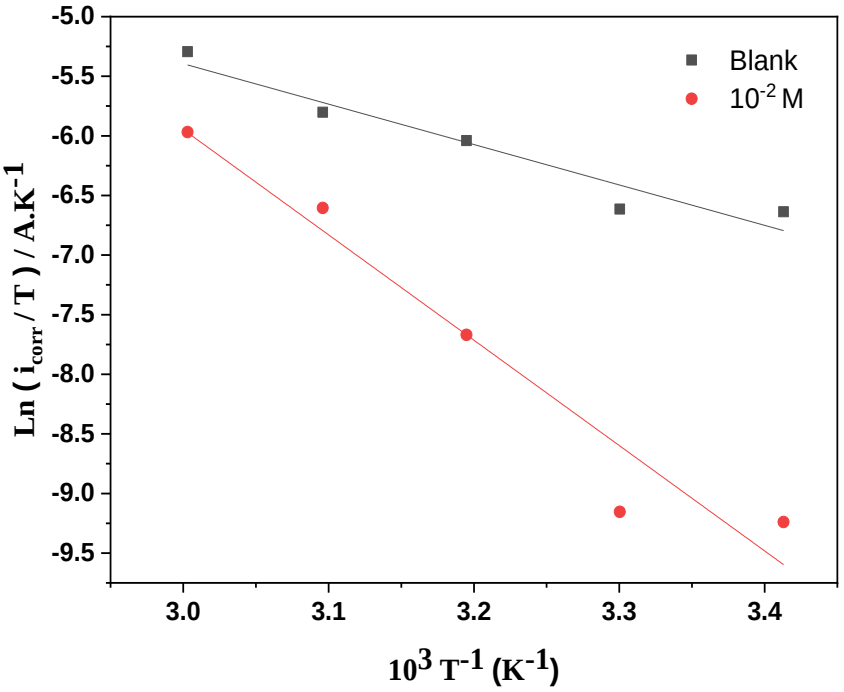

Figure 14. Transition state plots of Ln $I_{corr}/T = f(1/T)$ of Alloy 321 in 5.5 M phosphoric acid without and with the addition of 10^{-2} mol/L of AMHQ.

$\Delta S°_a$ and $\Delta H°_a$ values were obtained from the intercept (($\Delta S°_a$ /R) + Ln (R/Nh)) and the slope ($-\Delta H°_a/R$) of the straight lines of Ln $I_{corr}/T = f(1/T)$ plots. The obtained values are gathered and are given in Table 7.

The positive value of the enthalpy (ΔH_a) reveals that the dissolution of Alloy 321 in the studied conditions is an endothermic process. These results permit to verify the known relation between E_a and ΔH_a:

$$E_a - \Delta H_a = RT \qquad (14)$$

The calculated values in Table 7 ($E_a - \Delta H_a$) are close to RT (2.44 kJ/mol at 293 K), which is explained by the fact that the corrosion reaction is a unimolecular reaction. Negative entropy values (ΔS_a) imply a decrease in the disorder between the reagents and the formed complex. In other words, the activated compound in the rate-limiting step is obtained by an association of reagents, leading thus to more ordered elements. Furthermore, the adsorbed molecules lose their freedom of translation when they are adsorbed to the metal surface [43,44].

3.8. Computational Details

Quantum chemical methods have becoming a helpful tool for studying the corrosion inhibition of metals. Positive and negative regions on highest occupied (HOMO) and lowest unoccupied (LUMO) molecular orbitals of AMHQ in the ground state were computed by density functional theory (DFT) using B3LYP functional with 6-31G* basis set. This approach was chosen because of its high accuracy and reliability. It requires less computation time and offers similar precision for medium and large size

molecules.

Fig. 15 represents the optimized spatial geometry and the frontier molecular orbital density distribution of AMHQ molecule. Theoretical quantum parameters including molecular energy (E), energy of LUMO (E_{LUMO}), energy of HOMO (E_{HOMO}), dipole moment (μ) and energy band gap (ΔE) are summarized in Table 8.

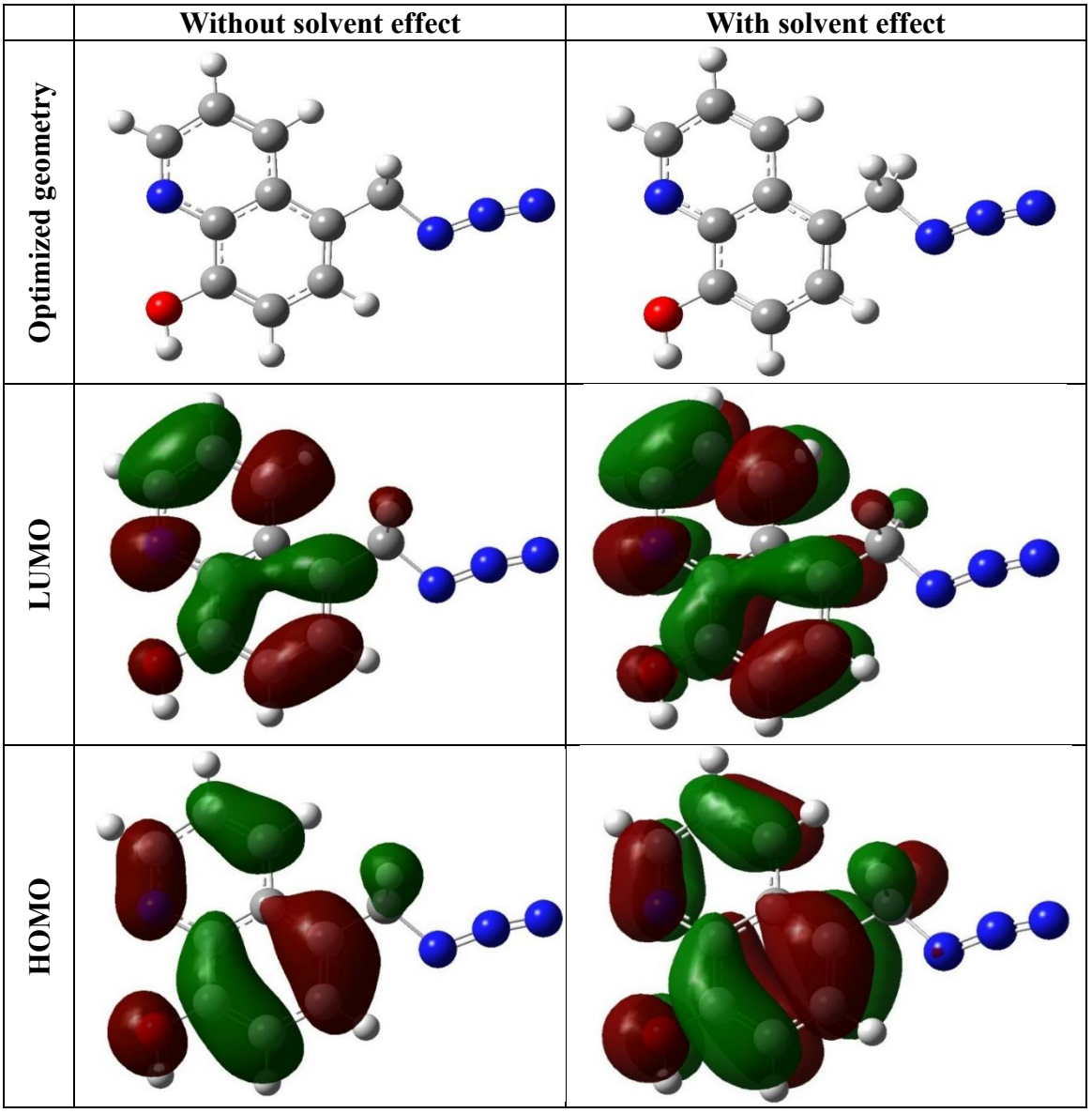

Figure 15. Frontier molecular orbital density distribution of AMHQ with and without solvent effect.

Inspection of E_{LUMO} and E_{HOMO} can theoretically explain the electronic properties of molecules. The positive green phases represent a growth in the electron density, while the negative red phases indicate a lowering in the electron density [45].

Table 8. Calculated quantum chemical parameters of AMHQ with and without solvent effect.

	Without solvent effect	**With solvent effect**
E (au)	-679.8	-679.8
E_{LUMO} (eV)	-1. 53	-1. 57
E_{HOMO} (eV)	-5.94	-5.97
ΔE (eV)	4.41	4.40
Dipole moment (Debye)	0.82	1.67

It is evident from Fig. 15 that AMHQ in aqueous phase has a quasi-planar structure, which involves a large surface covered by the inhibitors using relatively low concentrations. The estimated molecular energies in both phases are negative, indicating that AMHQ is thermodynamically stable in both gaseous and liquid phase. These values are almost identical and no solvent effect was observed on the stability of the molecule.

E_{HOMO} is usually taken as an indication of the ability of a compound to provide electrons to another suitable compound having an empty and low energy molecular orbital. The adsorption of inhibitors is favored for molecules with high E_{HOMO} through the transfer of electrons to the metal surface. [46,47]. Previous studies have shown that atomic sites with high density of the HOMO orbital are subjected to electrophilic attack, whereas atomic sites with high density of the LUMO orbital can undergo nucleophilic attacks [48,49]. E_{LUMO} reflects the tendency of a molecule to accept electrons. The lower the E_{LUMO} energy of the molecule, the higher its probability of receiving electrons from a donor compound [50,46,47]. The inhibitors can be adsorbed on metal surfaces by providing electrons from their highest occupied molecular orbitals, and also through the transfer of electrons from metals to their lowest unoccupied molecular orbitals involving the creation of a feedback bond [46,47].

Great values of E_{HOMO} indicate that AMHQ can easily provide electrons to an adequate acceptor with vacant molecular orbitals. However, E_{HOMO} has a negative sign that favors the physical adsorption of AMHQ on the metal surface rather than the chemisorption [51] in agreement with the result of the adsorption energy. It is worth pointing that high gap energy (ΔE) values imply high electronic stability and thus low reactivity, while low ΔE values mean that it will be easier to remove an electron from the HOMO to the LOMO orbitals leading to interesting inhibition performance [52]. ΔE values in Table 8 suggest that AMHQ has a strong tendency to adsorb on stainless steel corresponding to higher stability of the [SS–INHIBITOR] complex. On the other hand and according to the literature, the elevated inhibition efficiency of AMHQ can be related to the high dipole moment value due to the dipole-dipole interactions [51].

The LUMO and HOMO orbitals of AMHQ presented in Fig. 15 are localized around the oxygen atom and aromatic rings, which are the preferred molecule parts to interact with the alloy surface.

4. CONCLUSIONS

The objective of this study was to investigate the effect of 5-Azidomethyl-8-hydroxyquinoline (AMHQ) as a corrosion inhibitor of AISI 321 stainless steel (Alloy 321) in 5.5 M phosphoric acid

solution.

AMHQ acts as a mixed type corrosion inhibitor of Alloy 321 in 5.5 M phosphoric acid solution. The efficiency of AMHQ increases with increasing concentration and decrease with temperature. The inhibition action of AMHQ is explained by its adsorption on the stainless steel surface. The adsorption process is spontaneous and obeys to Langmuir adsorption isotherm. $\Delta G°_{ads}$ value implies a physisorption type interaction. Furthermore, activation energy of adsorption process decreases with the addition of AMHQ. Quantum chemical calculations were used to determine the optimal geometry of AMHQ, and to correlate the electronic properties of the molecule with corrosion inhibition performance.

The experiments conducted have shown a great efficiency for this synthetic inhibitor. It can be concluded that this molecule is a powerful anticorrosion agent that should be considered for industrial and wide uses.

ACKNOWLEDGEMENT
The authors acknowledge financial support of "National Center for Scientific and Technical Research" from Rabat-Morocco.

References

1. M. BenSalah, R. Sabot, E. Triki, L. Dhouibi, Ph. Refait and M. Jeannin, *Corros. Sci*., 86 (2014) 61.
2. S. Zor, M. Soncu and L. Aapan, *J. Alloys Compd*., 480 (2009) 885.
3. I.B. Obot, Z. M. Gasem, S.A. Umoren, *Int. J. Electrochem. Sci*., 9 (2014) 2367.
4. M.H. Mahros, Kürşat Efil, T.A. Seif El-Nasr and Osama A. Abbas, *J. Electrochem. Sci. Technol*., 8 (2017) 222.
5. Rola Y. Khaled and A. M. Abdel-Gaber, *Prot. Met. Phys. Chem. Sur*., 53 (2017) 956.
6. C. Excrivà-Cerdan, E. Blasco-Tamarit, D.M. García, J. García-Antón, R. Akid and J. Walton, *Electrochim. Acta*, 111 (2013) 552.
7. S Kitane, L Chraibi and M Soufiaoui, *Tetrahedron*, 48 (1992) 8935.
8. B. Himmi, D. Douche, A. El Louzi and K. Karrouchi, *J. Chem. Pharm. Res*., 8 (2016) 525.
9. H. Bougharraf, R. Benallal, T. Sahdane, D. Mondieig, Ph. Negrier, S. Massip, M. Elfaydy, B. Lakhrissi, and B. Kabouchi, *Russ. J. Phys. Chem*. A, 91(2017) 358.
10. Fadel Wedian, Mahmoud A. Al-Qudah and Ghassab M. Al-Mazaideh, *Int. J. Electrochem. Sci*., 12 (2017) 4664.
11. I. Ahamad, R. Prasad and M. Quraishi, *Corros. Sci.,* 52 (2010) 933.
12. Gökhan Gece, *Corros. Sci*., 50 (2008) 2981.
13. V. Kanagalasara and V.T. Venkatarangaiah, *Appl. Surf. Sci*., 257 (2011) 8929.
14. E.A. Abd El Meguid and A.A. Abd El Latif, *Corros. Sci*., 49 (2007) 263.
15. R. Solmaz, G. Kardas, B. Yazici and M. Erbil, *Coll. Surf. A Phys. Eng. Asp*., 312 (2008) 7.
16. M. A. Amin and M. M. Ibrahim, *Corros. Sci.,* 53 (2011) 873.
17. J.O'M. Bockris and A.K.N. Reddy, Modern Electrochemistry, Plenum Press, (1972) New York, USA.
18. E. Mc Cafferty, *Corros. Sci.,* 47 (2005) 3202.
19. W. Belmaghraoui, A. Mazkour, H. Harhar, M. Harir and S. El Hajjaji, *Anti-Corros. Methods Mater.,* 66 (2019) 121.
20. M. Shabani-Nooshabadi, and M.S. Ghandchi, *J. Ind. Eng. Chem.,* 31 (2015) 231.
21. F. Bouhlal, N. Labjar, F. Abdoun, A. Mazkour, M. Serghini-Idrissi, M. El Mahi, E. M. Lotfi, A. Skalli and S. El Hajjaji, *Egypt. J. Pet.,* 29 (2020) 45.
22. O. Kaczerewska, R. Akid, B. Brycki, I. Kowalczyk, and T. Pospieszny, *J. Mol. Liq.,* 249 (2018) 1113.

23. A. Ehsani, R. Moshrefi and M. Ahmadi, *J. Electrochem. Sci. Technol*., 6 (2015) 7.
24. Z. Lukacs, *J. Electroanal. Chem*., 432 (1997) 79.
25. V. Maurice, W.P. Yang and P. Marcus*, J. Electrochem. Soc*., 145 (1998) 909.
26. I. Olefjord and B.O. Eflström, *Corrosion*, 38 (1982) 46.
27. B. Hirschorn, M. E. Orazem, B. Tribollet, V. Vivier, I. Frateur et M. Musiani, *Electrochim. Acta*, 55 (2010) 6218.
28. M.E. Orazem, I. Frateur, B. Tribollet, V. Vivier, S. Marcelin, N. Pébère, A.L.Bunge, E.A. White, D.P. Riemer and M. Musiani, *J. Electrochem. Soc.*, 160 (2013) 215.
29. V.M.-W. Huang, V. Vivier, I. Frateur, M.E. Orazem and B. Tribollet, *J. Electrochem. Soc*., 154 (2007) 89.
30. T.L. Sudesh, L. Wijesinghe, D.J. Blackwood, *J. Electrochem. Soc*., 153 (2006) 178.
31. Z. Feng, X. Cheng, Ch. Dong, L. Xu and X. Li, *Corros. Sci*., 52 (2010) 3646.
32. M. Ben Salah, R. Sabot, Ph. Refait, I. Liascukiene, C. Méthivier, J. Landoulsi, L. Dhouibi et M. Jeannin, *Corros. Sci*., 99 (2015) 320.
33. S. Vikneshvaran, S. Velmathi, *Surf. Interfaces,* 6 (2017) 134.
34. Ebenso, E.E.; Eddy, N.O. and Odiongenyi, A.O., *Port. Electrochim. Acta*, 27 (2009) 13.
35. A. AliAnejjar, R. Salghi, A. Zarrouk, H. Zarrok, O. Benali, B. Hammouti, S.S. Al-Deyab, N.E. Benchat and R. Saddik, *Res. Chem. Intermed*., 41 (2015) 913.
36. M.H. Hussin and M. Kassim, *J. Mater. Chem. Phys*., 125 (2011) 461.
37. P. Mourya, S. Banerjee, R.B. Rastogi and M.M. Singh, *Ind. Eng. Chem. Res*., 52 (2013) 12733.
38. M. Scendo and K. Staszewska-samson, *Int. J. Electrochem. Sci*., 12 (2017) 5668.
39. A. K. Satpati, M. M. Palrecha and R. I. Sundaresan, *Indian J. Chem. Technol*., 15 (2008) 163.
40. Robert G. Kelly, John R. Scully, David w. Shoesmith, Rudolph G. Buchheit, Elecrochemical techniques in corrosion science and engineering, Marcel Dekker, Inc., 2002 New York, USA.
41. T. Poornima, J. Nayak, and A. N. Shetty, *Chem. Sci.* J., 69 (2012) 14.
42. T. Szauer and A. Brand, *Electrochim. Acta*. 26 (1981) 1219.
43. M. Behpour, S.M. Ghoreishi, M. Khayatkashani and N. Soltani, *Corros. Sci*., 53 (201) 2489.
44. R. Solmaz, G. Kardas_, M. Culha, B. Yazıcı and M. Erbil, *Electrochim. Acta*. 53 (2008) 5941.
45. K. Laxmi, *J. Appl. Chem*., 2 (2014) 92.
46. N. Soltani, N. Tavakkoli, M. Khayatkashani, M.R. Jalali and A. Mosavizade, *Corros. Sci.,* 62 (2012) 122.
47. I. B. Obot, Z. M. Gasem, S. A. Umoren, *Int. J. Electrochem. Sci*., 9 (2014) 510.
48. B. Adindu, C. Ogukwe, F. Eze and E. Oguzie*, J. Electrochem. Sci. Technol*., 7 (2016) 251.
49. Swayansiddha Tripathy and Susanta KumarSahu, *Int. J. Pharma. Sci.,* 6 (2016) 1534.
50. A.Y. Musa, W. Ahmoda, A.A. Al-Amiery, A.A.H. Kadhum and A.B. Mohamad, *J. Struct. Chem*., 54 (2013) 301.
51. I. Belfilali, A. Chetouani, B. Hammouti, S. Louhibi, and A. Aouniti, *Res. Chem. Intermed.,* 40 (2014) 1069.
52. H. Elmsellem, H. Nacer, F. Halaimia, A. Aouniti, I. Lakehal, A .Chekjjltouani, S. S. Al-Deyab, I. Warad, R. Touzani and B. Hammouti, *Int. J. Electrochem. Sci*., 9 (2014) 5328.